Is There a Covalent Intermediate in the Viral Neuraminidase Reaction? A Hybrid Potential Free-Energy Study

Aline Thomas, David Jourand, Celine Bret, Patricia Amara, and Martin J. Field*

Contribution from the Laboratoire de Dynamique Moléculaire, Institut de Biologie Structurale—Jean-Pierre Ebel, 41, rue Jules Horowitz, F-38027 Grenoble Cedex 01, France

Received May 13, 1999

Abstract: The neuraminidase from the influenza virus is essential for maintaining viral infectivity as it aids in the transmission of the virus between cells. Although there are large variations in the amino acid sequences of neuraminidases from different influenza strains, there are several amino acids in the active site region of the protein that are strictly conserved. This has raised hopes that a single neuraminidase inhibitor and, hence a drug, can be found that is effective against all influenza strains. In this paper, we examine with theoretical simulation techniques one aspect of the reaction catalyzed by the viral neuraminidase that could be important for inhibitor design studies—namely, whether a covalently bound complex can be formed between the enzyme and the sialosyl cation intermediate that occurs during the reaction. We used a hybrid semiempirical quantum mechanical/molecular mechanical (QM/MM) potential in conjunction with potential of mean force calculations to determine the free-energy profiles for formation of the covalent intermediate and its hydrolysis to sialic acid and for the direct hydroxylation of the sialosyl cation to sialic acid. Ab initio QM calculations were used to check the validity of the semiempirical results. We find that direct hydroxylation of the sialosyl cation is the energetically preferred pathway but not by so much that the possibility of being able to design covalently bound inhibitors need be completely abandoned.

Introduction

Neuraminidases are ubiquitous enzymes. They are present in viruses, bacteria, and parasites and they have been implicated in serious diseases such as pneumonia, cholera, and meningitis. In the influenza virus, neuraminidases, like the viral hemagglutinin proteins, are bound to the membrane at the surface of the virus where they can cleave the terminal sialic acids of glycolipids and of glycoproteins (see Figure 1). This reaction is important because it prevents the virus from getting trapped by glycoprotein receptors binding to its hemagglutinins and so enhances its spread from the surface of infected cells. It also enables the penetration of the virus into the sialic acid-rich mucosal secretions up to the respiratory epithelium and prevents aggregation of the virus on the surface of infected cells (for reviews, see refs 1−3). Because of the ever-present threat of an outbreak of a new and potentially virulent strain of influenza and the critical role played by neuraminidases in the life cycle of the virus, there has been a great deal of interest in the design of inhibitors of neuraminidase that could act as anti-influenza drugs[4−9] even though "inhibitor pressure" stimulates in vitro
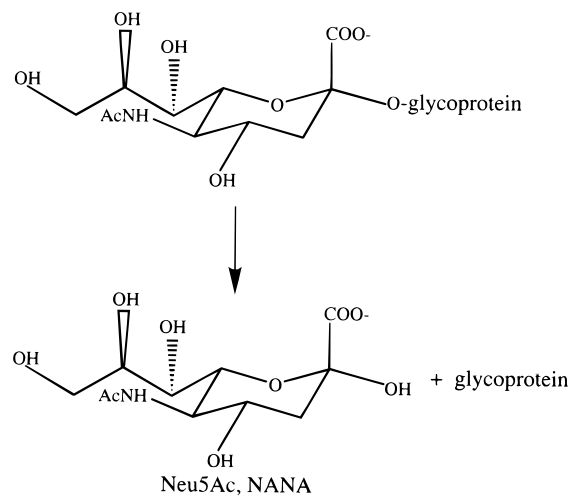

Figure 1. Schematic diagram of the reaction catalyzed by neuraminidases. NANA and Neu5Ac stand for *N*-acetylneuraminic acid.

the emergence of new resistant influenza strains.[10−13] Several neuraminidase inhibitors are currently clinically prescribed (e.g., Rimantidine and Amantidine) or are undergoing clinical trials (e.g., Zanamivir).

* Corresponding author: (tel) (33)-4-76-88-95-94; (fax) (33)-4-76-88-54-94; (e-mail) thomas@ibs.fr and mjfield@ibs.fr.

(1) Air, G. M.; Laver, W. G. *Proteins: Struct. Funct. Genet.* **1989**, *6*, 341−56.

(2) Colman, P. M. *Protein Sci.* **1994**, *3*, 1687−96.

(3) Taylor, G. *Curr. Opin. Struct. Biol.* **1996**, *6*, 830−7.

(4) Wade, R. C. *Structure* **1997**, *5*, 1139−45.

(5) Service, R. F. *Science* **1997**, *275*, 756−7.

(6) Kim, C. U.; Lew, W.; Williams, M. A.; Liu, H.; Zhang, L.; Swaminathan, S.; Bischofberger, N.; Chen, S. M.; Mendel, D. B.; Tai, C. Y.; Laver, W. G.; Stevens, R. C. *J. Am. Chem. Soc.* **1997**, *119*, 681−90.

(7) Kati, W. M.; Salvidar, A. S.; Mohamadi, F.; Sham, H. L.; Laver, W. G.; Kohlbrenner, W. E. *Biochem. Biophys. Res. Commun.* **1998**, *244*, 408−18.

(8) Jedrzejas, M. J.; Singh, S.; Brouillette, W. J.; Laver, W. G.; Air, G. M.; Luo, M. *Biochemistry* **1995**, *34*, 3144−51.

(9) Williams, M. A.; Lew, W.; Mendel, D. B.; Tai, C. Y.; Escarpe, P. A.; Laver, W. G.; Stevens, R. C.; Kim, C. U. *Bioorg. Med. Chem. Lett.* **1997**, *7*, 1837−42.

(10) Varghese, J. N.; Smith, P. W.; Sollis, S. L.; Blick, T. J.; Sahasrabudhe, A.; McKimm-Breschkin, J. L.; Colman, P. M. *Structure* **1998**, *6*, 735−46.

(11) Sahasrabudhe, A.; Lawrence, L.; Epa, V. C.; Varghese, J. N.; Colman, P. M.; McKimm-Breschkin, J. L. *Virology* **1998**, *247*, 14−21.

(12) Blick, T. J.; Sahasrabudhe, A.; McDonald, M.; Owens, I. J.; Morley, P. J.; Fenton, R. J.; McKimm-Breschkin, J. L. *Virology* **1998**, *246*, 95−103.

(13) Gubareva, L. V.; Robinson, M. J.; Bethell, R. C.; Webster, R. G. *J. Virol.* **1997**, *71*, 3385−90.
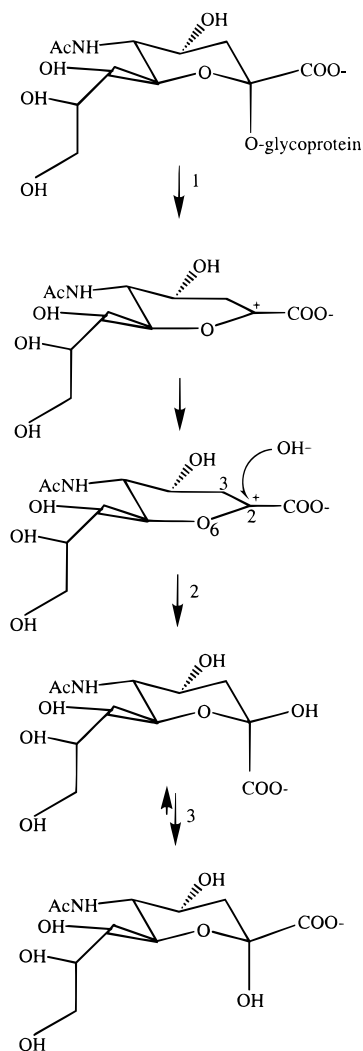
Figure 2. Schematic diagram of a possible mechanism for the neuraminidase reaction. Step 1 leads to the sialosyl cation (or the oxocarbonium) intermediate, step 2 leads to the formation of the α sialic acid, and step 3 is the mutarotation that produces the β-anomer.

There are numerous crystal structures available for neuraminidases from different species, both alone and when complexed with monoclonal antibodies, with the reaction product and with various inhibitors. Even though all influenza virus neuraminidases share only ~30% of their sequence identity, they have a highly conserved folding pattern. Each neuraminidase is a homotetramer in which the monomers contain ~390 residues and are folded into six four-stranded antiparallel β-sheets that are arranged like the blades of a propeller. Among the 9 serological subtypes of the type A virus and the single subtype of the type B virus, 11 of the residues lining the active site are strictly conserved.[14] The reaction mechanism hypothesized to take place in this shallow pocket is shown in Figure 2. In the first step, the sialyl substrate binds to the enzyme and its pyranose ring is distorted by the highly charged environment of the active site from the chair conformation that is preferred in solution into an α-boat conformation. This unfavorable conformation, in which the C2, C3, and O6 atoms are coplanar, also occurs in the sugar substrate that binds to another glycosidase, lyzozyme. The resulting conformational strain induces the cleavage of the glycosidic bond, the departure of the attached sugar, and the formation of an oxocarbonium ion

intermediate that has been identified by kinetic isotope effect experiments.[15,16] The second step in the reaction is the hydroxylation of the C2 atom of the intermediate by a water molecule that has been activated by an aspartic acid residue. In the third and last step, the α-sialic acid is released with retention of configuration at the C2 atom. Mutarotation at this atom can then take place in the solvent.

The stabilization of the positive charge of the sialosyl cation intermediate has been the subject of some discussion. Some authors have supposed that it is due to the side-chain oxygen atom of an active site tyrosine that is close to the C2 atom of the intermediate and whose phenolate character could be enhanced by hydrogen bonding to a neighboring glutamate residue.[17] This tyrosine is crucial for catalysis because a recent site-directed mutagenesis study shows that mutation of the tyrosine to a phenylalanine completely abolishes the enzymatic activity.[18] However, this hypothesis has been challenged since at the optimum pH for the enzyme, ~6, tyrosine is protonated.[15,16] Another possibility is that the active site directly stabilizes the planar conformation of the oxocarbonium intermediate rather than employing nucleophilic or proton donation effects.[19] A third alternative, which appears to have been ruled out experimentally,[15,20] is the formation of a covalent intermediate with the enzyme.

Some years ago, in a theoretical study of the reaction mechanism of the viral neuraminidase in our laboratory,[21] it quickly became clear with the theoretical model we were using that it was possible, at a relatively low energetic cost, for the tyrosine in the active site to form a covalent bond with the oxocarbonium C2 atom while passing on its hydrogen to an adjacent glutamate residue. Because of the important mechanistic implications of this result and the possibilities that it could engender for the design of anti-influenza drugs, we decided to investigate in more detail this particular aspect of the neuraminidase reaction.

In both our original and the current work, we employed a hybrid quantum mechanical (QM)/molecular mechanical (MM) potential as the energy function in our simulations. The concept underlying such hybrid potentials is that the system is partitioned into a small region that is treated quantum mechanically and in which the bond breaking and bond formation occurs and the rest of the system that is treated with molecular mechanics and that acts as the environment of the QM region. Such potentials have been shown to be very useful for studying reaction processes in the condensed phase, and to date, more than 20 studies of enzymatic reaction mechanisms using QM/MM potentials have been published (for a review see ref 22). In the great majority of these studies, the reaction paths were investigated using energy minimization or, to a lesser extent, saddle point location techniques. These QM/MM reaction path-type approaches have already been tried on neuraminidase bound to a *p*-nitrophenyl-*N*-acetylneuraminide substrate[20] and to the

(14) Colman, P. M.; Hoyne, P. A.; Lawrence, M. C. *J. Virol.* **1993**, *67*, 2972−80.

(15) Chong, A. K. J.; Pegg, M. S.; Taylor, N. R.; von Itzstein, M. *Eur. J. Biochem.* **1992**, *207*, 335−43.

(16) Taylor, N. R.; von Itzstein, M. *J. Med. Chem.* **1994**, *37*, 616−24.

(17) Burmeister, W. P.; Henrissat, B.; Bosso, C.; Cusack, S; Ruigrok, R. W. H. *Structure* **1993**, *1*, 19−26.

(18) Ghate, A. A.; Air, Q. M. *Eur. J. Biochem.* **1998**, *258*, 320−31.

(19) Janakiraman, M. N.; White, C. L.; Laver, W. G.; Air, G. M.; Luo, M. *Biochemistry* **1994**, *33*, 8172−9.

(20) Barnes, J. A.; Williams, I. H. *Biochem. Soc. Trans.* **1996**, *24*, 263−8.

(21) Jourand, D. *Etude théorique du mécanisme réactionnel de la neuraminidase d'influenza B. Conception d'un algorithme de drug design.* Thèse, de l'Université Joseph Fourier, Grenoble, France 1998.

(22) Amara, P.; Field, M. J. *Computational Molecular Biology*; Leszczynski, J., Ed.; Elsevier Science: Amsterdam, 1999; pp 1−33.

natural substrate.[21] In the first study, the theoretical kinetic isotope effects were computed from the reaction energy surface, but they were not totally in agreement with the experimental data, whereas the second study, as mentioned above, postulated the existence of a covalent bond between the C2 atom of the intermediate and the side-chain oxygen of the active site tyrosine.

While the calculation of reaction paths using minimization-type approaches is useful, it is the free energy that is the quantity of primary interest when reaction processes are investigated. Thus, in this work, we have preferred to calculate the free-energy profiles for two possible pathways in the neuraminidase reaction that lead from the sialosyl cation to the sialic acid product. Such free-energy calculations represent the state of the art in the application of QM/MM hybrid potential techniques.[23−25]

The outline of this paper is as follows. The next section describes the details of our computational methods, followed by the results of the calculations, and then the conclusion.

Computational Details

1. Setting Up the Simulations. Of the many crystallographic structures of neuraminidase that are available, we selected structure 1NSD from the Brookhaven Protein Data Bank.[26] This is the neuraminidase from influenza virus strain B/Beijing/1/87 complexed with the 2-deoxy-2,3-dihydro-*N*-acetylneuraminic acid (DANA) and solved at 1.8-Å resolution.[27] DANA is an inhibitor that is synthesized by the enzyme itself in a suicide reaction that leads to the formation of a double bond between the atoms C2 and C3.[17] It should be remarked, however, that a recent study has indicated that the hydration of DANA by neuraminidase is reversible.[19] A global view of the active site/DANA complex, together with distances involving residues important for the stabilization of DANA in the 1NSD coordinate set, is shown in Figure 3. Most of the residues lining the active site are charged. The carboxylate oxygens on the C1 atom of DANA have hydrogen bonds to the arginines R115, R373, and R467, whereas the hydroxyl hydrogens of O8 and O9 interact with the side-chain carboxylate oxygens of glutamate E274. O8 itself is hydrogen-bonded to the side chain of R222 and the carbonyl oxygen, O10, to the side chain of R149. A hydrogen bond that will be important in our later discussions occurs between residues of the protein and is the one involving the side-chain carboxylate oxygens of E275 and the hydrogen atom of tyrosine Y408.

In our calculations, we used two different molecular modeling programs. Most of the simulations were done with the DY-NAMO program,[28] but some of our earlier calculations were performed with the CHARMM program.[29] All the calculations in our initial study of neuraminidase[21] used CHARMM. Although two different programs were employed, our basic approach was similar for both. In each case, we used a hybrid
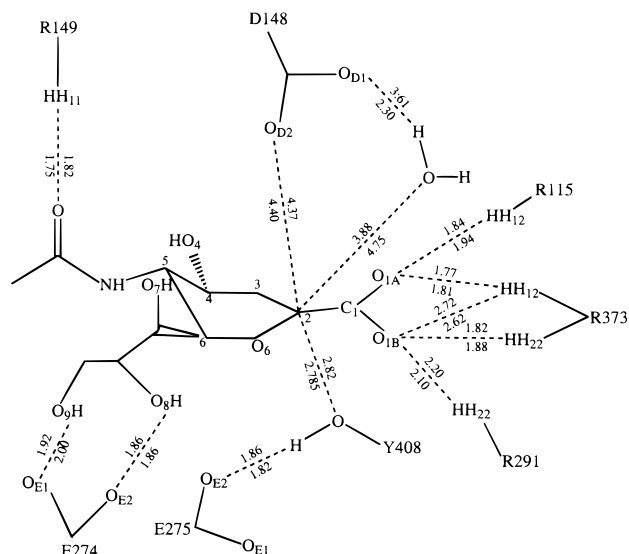

Figure 3. Representation of the DANA/active site complex in the 1NSD PDB structure.[27] Important distances (in Å) are given for each of the two monomers present in the asymmetric unit. DANA (or Neu5Ac2en) stands for 2-deoxy-2,3-dehydro-*N*-acetylneuraminic acid.

QM/MM potential of the type described in ref 30. The AM1 semiempirical method was employed as the QM potential[31,32] and an all-atom force field for the MM potential—the new all-atom force field[33] for CHARMM and the OPLS-AA force field in DYNAMO.[34]

We selected a single monomer of the neuraminidase for our simulations—the distance between the active sites of the protein is large, more than 40 Å, and there is no evidence for any functional coupling between them. The first step in our studies was the construction of the missing coordinates in the structure. Owing to the planarity about its C2 atom, DANA strongly resembles the oxocarbonium intermediate and so we modeled the structure of the latter from it. The coordinates of all the missing hydrogen atoms in the enzyme were then added using the HBUILD algorithm[35] in CHARMM and refined using a short geometry optimization. To solvate the protein, a cubic box of water molecules, thermalized at 300 K and of side 70 Å, was superimposed upon the system. All water molecules overlapping with atoms of the protein/cation complex were then removed, and a geometry optimization was performed. The process of superposition and optimization was continued until no more water molecules could be added. As the final step in the preparation, we centered the system at the midpoint between the C2 atom of the intermediate and the oxygen of Y408 and deleted all atoms further away than 35 Å. This left ~16 000 atoms in total including all the protein atoms and one to two solvation layers at the protein's surface.

(23) Liu, H.; Muller-Plathe, F.; van Gunsteren, W. *J. Mol. Biol.* **1996**, *261*, 454−69.

(24) Alhambra, C.; Wu, L.; Zhang, Z.-Y.; Gao, J. *J. Am. Chem. Soc.* **1998**, *120*, 3858-66.

(25) Bentzien, J.; Müller, R. P.; Florián, J.; Warshel, A. *J. Phys. Chem. B* **1998**, *102*, 2293−301.

(26) Bernstein, F. C.; Koetle, T. F.; Williams, G. J. B.; Meyer, E. F.; Brice, M. D.; Rodgers, J. R.; Kennard, O.; Shimanouchi, T.; Tasumi, M. *J. Mol. Biol.* **1977**, *112*, 535−42.

(27) Burmeister, W. P.; Ruigrok, R. W. H.; Cusack, S. *EMBO J.* **1992**, *11*, 49−56.

(28) Field, M. J.; Amara, P.; Bret, C.; Proust, F.; Thomas, A. To be published.

(29) Brooks, B. R.; Bruccoleri, R. E.; Olafson, B. D.; States, D. J.; Swaminanathan, S.; Karplus, M. *J. Comput. Chem.* **1983**, *4*, 187−217.

(30) Field, M. J.; Bash, P. A.; Karplus, M. *J. Comput. Chem.* **1990**, *11*, 700−33.

(31) Dewar, M. J. S.; Zoebisch, E. G.; Healy, E. F.; Stewart, J. J. P. *J. Am. Chem. Soc.* **1985**, *107*, 3902−9.

(32) Dewar, M. J. S.; Dieter, K. M. *J. Am. Chem. Soc.* **1986**, *108*, 8075−86.

(33) Mackerell, A. D., Jr; Bashford, D.; Bellott, M.; Dunbrack, R. L., Jr; Evanseck, J. D.; Field, M. J.; Fischer, S.; Gao, J.; Guo, H.; Ha, S.; Joseph-McCarthy, D.; Kuchnir, L.; Kuczera, K.; Lau, F. T. K.; Mattos, C.; Michnick, S.; Ngo, T.; Nguyen, D. T.; Prodhom, B.; Reiher, W. E., III; Roux, B.; Schlenkrich, M.; Smith, J. C.; Stote, R.; Straub, J. E.; Watanabe, M.; Wiórkiewicz-Kusczera, J.; Yin, D.; Karplus, M. *J. Phys. Chem. B* **1998**, *102*, 3586−616.

(34) Jorgensen, W. L.; Maxwell, D. S.; Tirado-Rives, J. *J. Am. Chem. Soc.* **1996**, *118*, 11225−36.

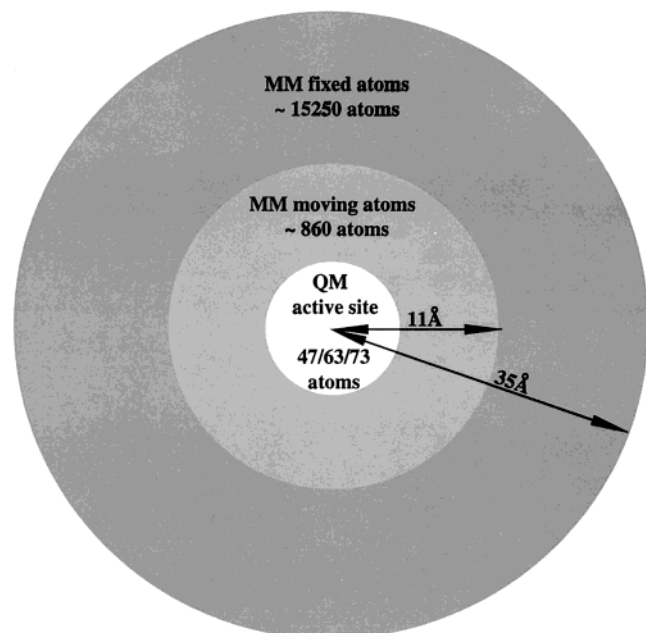(35) Brünger, A. T.; Karplus, M. *Proteins: Struct. Funct. Genet.* **1988**, *4*, 148−56.

Figure 4. Schematic diagram of how the hybrid potential simulation system was partitioned into different regions. The QM region contained 47, 63, or 73 atoms, depending upon the reaction being studied, whereas the inner MM region, that contained atoms free to move, had ~860 atoms.

In all our QM/MM simulations, the system described above was divided into three zones as indicated in Figure 4. The QM region, in which the reacting atoms are modeled, contained the sialosyl cation, one or more of the side chains of the residues D148 (an aspartate), E275 and Y408, and possibly a water molecule. The number of atoms treated quantum mechanically varied depending upon the stage of the reaction being studied, but we employed models in which there were 47, 63, and 73 QM atoms. These are shown in Figure 5. The remainder of the atoms were treated with an MM potential but we divided them into two sets—those close to the QM region, which were allowed to move in our simulations, and those further away, which were fixed but which could interact with the QM and MM atoms in the central zones. The moving MM atoms were defined as those that were within a sphere of 11-Å radius centered midway between the cation C2 atom and the oxygen of Y408 and contained ~860 atoms.

As is normal when studying enzyme reaction mechanisms with QM/MM potentials, a part of the protein is in the QM region and a part in the MM region. To cope with the covalent bonds between the atoms of the QM and MM regions we used the dummy or link-atom approximation, which has been fully explained in refs 30 and 36. Thus, for each covalent bond between the two regions we placed a QM hydrogen atom, invisible to the atoms in the MM region, at ~1 Å from the QM atom at the boundary of the QM region and pointing toward the MM atom at the other end of the covalent bond. The link atom enters into the QM calculation in the normal way and is free to move in the simulations while the covalent interactions between the QM and MM atoms at the boundary is described with the appropriate terms in the force field.[30] Depending upon the stage of the reaction that we were studying, link atoms were introduced for the side chains of residues D148, E275, and Y408 between the Cβ atom of the QM region and the Cα atom of the MM region.

2. The Hybrid Potential Simulations. Whenever preparing the system for a particular simulation, i.e., using a different QM/

(36) Singh, U. C.; Kollman, P. A. *J. Comput. Chem.* **1986**, *7*, 718–30.
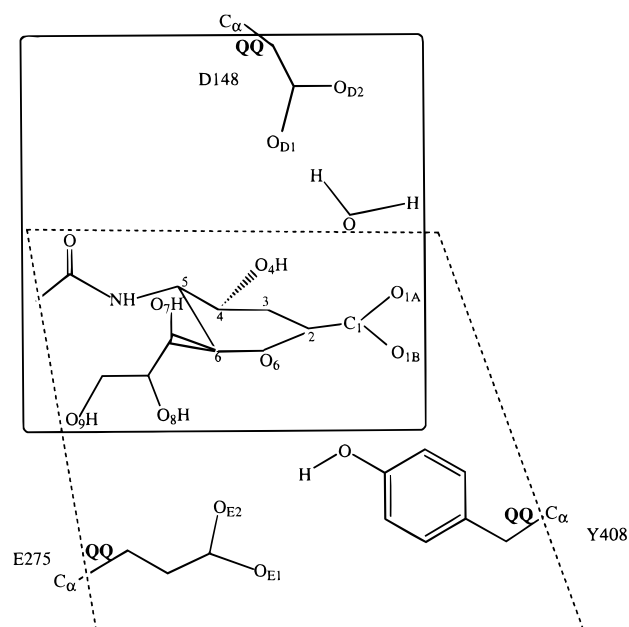

Figure 5. Schematic diagram of the three different QM regions that we used in our simulations. The 47 QM atom active site is within the solid box, the 63 QM atom active site is within the dotted box, and the 73 QM atom active site contains all the atoms within the solid and dotted box. Note that the link atoms are labeled as "QQ" and the Cα atoms of the amino acid residue side chains are always in the MM region.

MM partitioning or a different force field, we followed the same basic procedure. This consisted of a short minimization of the QM and MM atoms that were free to move, using either an adopted basis set Newton–Raphson algorithm (in CHARMM) or a conjugate-gradient method (in DYNAMO), followed by a short molecular dynamics simulation at 300 K. In all the simulations, the distances between the reacting atoms were harmonically constrained to have the same values as those in the crystal structure. All molecular dynamics simulations were done with a Langevin algorithm using a friction coefficient of 10^{-1} ps for each atom and a time step of 1 fs. The QM/MM and MM/MM nonbonding interactions were calculated using a group-based switching truncation function with inner and outer cutoffs of 9.5 and 13.5 Å, respectively, in CHARMM and an atom-based force-switching truncation function, with the same inner and outer cutoffs, in DYNAMO.[28,37] Using the results of some of our later calculations, we were able to show that these cutoffs gave essentially equivalent results (in this case) to calculations in which no truncation approximation was used.

The first simulation that we performed was a straightforward free molecular dynamics simulation, with CHARMM, to see how the system evolved without constraints. This simulation was done with 63 atoms in the QM region, i.e., the intermediate and the side chains of E275 and Y408. For the remainder of our simulations, which used DYNAMO, we determined the free energies along various appropriately chosen reaction coordinates by calculating the potential of mean force[38] using the method of umbrella sampling.[39,40] To do this, we employed the following strategy:

1. Choose a reaction coordinate as functions of one or more coordinates, ξ_1, ξ_2, ..., in the system. In most cases, we chose

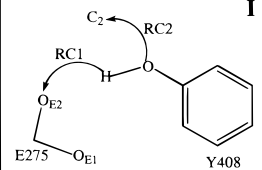(37) Steinbach, P. J.; Brooks, B. R. *J. Comput. Chem.* **1994**, *15*, 667–83.
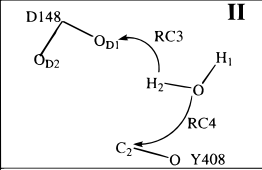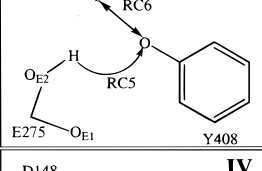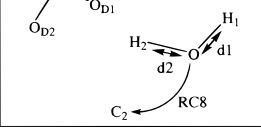
(38) Kirkwood, J. G. *J. Chem. Phys.* **1935**, *3*, 300.

(39) Valleau, J. P.; Torrie, G. M. *Statistical Mechanics*; Berne, B. J., Ed.; Plenum Press: New York, 1977; Part A, pp 169–194.

(40) Torrie, G. M.; Valleau, J. P. *Chem. Phys. Lett.* **1974**, *28*, 578–81.

Table 1. Details of the QM/MM Free-Energy Simulations[a]

QM Region	Reaction	Reaction Coordinates	Simulation	$\Delta G^\ddagger$	ΔG
63 atoms	**I**	RC1 = OE2 ... H RC2 = O ... C2	Step (a) RC1 = [0.9,2.0] RC2 = 2.785 Step (b) RC1 = 0.97 RC2 = [1.2,2.9]	+22 (+16) 0	-121
73 atoms	**II**	RC3 = H2 ... OD1 RC4 = O ... C2	Steps (c) and (d) RC3 = [0.9,2.15] RC4 = [1.4,2.4]	+110	0
73 atoms	**III**	RC5 = H ... O RC6 = O ... C2	Step (e) RC5 = [0.9,2.0] RC6 = 2.4	+40	+9
47 atoms	**IV**	RC7 = d₁ + d₂ RC8 = O ... C2	Steps (f) and (g) RC7 = [1.98,3.48] RC8 = [1.2,2.5]	+12	-97

[a] For each reaction step, the number and the identity of the atoms in the QM region are defined, as are the reaction coordinates and the ranges over which they are calculated. Also given are values obtained for the free-energy barriers, $\Delta G^\ddagger$, and the free-energy differences, ΔG. All distances are in angstroms and energies in kilojoules per mole. The free-energy calculations were done in all cases with windows separated by 0.05 Å, except for the case of RC4, where a step of 0.2 Å was found adequate. The free-energy barrier value in brackets for step a of reaction I is the path integral simulation result.

simple distances between atoms as functions, i.e., $\xi = d_{ij}$, where d_{ij} is the distance between atoms i and j, but in one case we chose a sum of two distances, i.e., $\xi = d_{ij} + d_{ik}$.

2. Define umbrella potentials, v_i, for each of the coordinates, ξ_i. In all cases we took a harmonic form:

$$v_i(\xi_i) = \frac{1}{2} k_i(\xi_i - \xi_i^0)^2 \qquad (1)$$

where k_i is the force constant for the potential and ξ_i^0 is a constant reference value for the coordinate.

3. Perform a series of molecular dynamics simulations for the system in the presence of the umbrella potentials. The simulations are the same except that they are performed with different reference values of the reaction coordinate, ξ_i^0, in the umbrella potentials. The aim is to have the simulations sample the complete range of values of the ξ_i for which a free-energy profile is required. For the free-energy profile to be reasonable, it is also necessary that simulations with neighboring umbrella potential reference values sample regions of the reaction coordinate that overlap to some extent. In practice, we found that using a force constant of 2000 kJ mol⁻¹ Å⁻² for the umbrella potentials and reference values that differed by 0.05 Å between windows was adequate. To obtain converged PMFs, it was necessary to run the simulations for each window for ∼10 ps with at least 0.5 ps of equilibration.

4. At each step of the data collection phases of the simulations, save the actual values of the coordinates, ξ_i, on an external file.

Once the reaction-coordinate data were collected from the simulations, the reaction-coordinate distribution functions were determined for each window and then pieced together using

the weighted histogram analysis (WHAM) method.[41] The resulting "unbiased" distribution function, $\langle\rho(\xi_1, ...)\rangle$, was then used to calculate the PMF, W, from

$$W(\xi_1, ...) = c - k_B T \ln \langle\rho(\xi_1, ...)\rangle \qquad (2)$$

where k_B is Boltzmann's constant, T is the temperature, and c is an arbitrary additive constant. As has been reported elsewhere,[42] we found the WHAM method to be a reliable way of extracting free-energy profiles in one or more dimensions.

Full details of all the free-energy calculations performed together with the QM/MM partitioning, the definition of the reaction coordinates, and the resulting free-energy values are given in Table 1. The formation of the sialic acid from the oxocarbonium intermediate was simulated via the formation of a covalent bond with Y408, reactions I−III, or by direct attack by a water molecule, reaction IV. We explored quite a few different possible schemes for each of these pathways, and the results we present in Table 1 are a synthesis of the lowest energy pathways that we found.

The production of sialic acid via the formation of the covalent intermediate, reactions I−III, can be decomposed into the following steps: (a) departure of the hydrogen from the side chain of Y408 to the side-chain oxygen of E275; (b) binding of the deprotonated Y408 phenolate anion to the C2 atom of the intermediate; (c) capture of the water hydrogen by one of the carboxylate oxygens of D148; (d) attack of the hydroxyl ion on the C2 atom of the covalent intermediate; (e) back protonation of Y408 from E275.

(41) Kumar, S.; Bouzida, D.; Swendsen, R. H.; Kollman, P. A.; Rosenberg, J. M. *J. Comput. Chem.* **1992**, *13*, 1011−21.

(42) Roux, B. *Comput. Chem. Commun.* **1995**, *91*, 275−82.

The formation of the oxocarbonium intermediate without the formation of the phenolate anion occurs via steps similar to those of (c) and (d) in reaction II. We label them steps f and g. In Table 1, steps a and b are grouped as reaction I, steps c and d as reaction II, and steps f and g as reaction IV. As will be discussed below, the lowest energy pathway for reaction I had steps a and b occurring consecutively whereas reaction II and, to some extent, reaction IV involved concerted changes of the reaction coordinates defining steps c and d and steps f and g, respectively.

All calculations were done on PC/Linux-based systems and up to 60 processors on a Cray T3E parallel machine at the CEA computer center in Grenoble. On the CRAY, 1 ps of dynamics of our simulation system with 73 atoms in the QM region took ∼2 h on a single processor. All our free-energy calculations were perfectly parallelizable because the simulations for separate windows were run simultaneously and independently on separate processors.

3. Path Integral Simulations. It is well known that the neglect of quantum dynamical effects can have an important effect when reactions are studied, particularly those involving hydrogens. To estimate the magnitude of this effect, we developed a path integral algorithm for use with hybrid QM/MM potentials in DYNAMO and then applied it to calculating the PMF for step a of reaction I. Full details of this approach along with a discussion of the problems that can arise when such simulations are done will be given elsewhere, and so only a brief summary will be presented here.[28]

In the path integral approach to obtaining quantum equilibrium properties, a classical simulation is performed with a potential derived by considering the isomorphism that exists between a discretized Feynman path integral representation of the equilibrium QM density operator and a classical system in which the quantum particles are represented by polymers of classical particles.[43,44] The form of the effective potential is as follows:

$$
\mathcal{W}_{PI} = \sum_{i=1}^{N_Q} \frac{P m_i (k_B T)^2}{2\hbar^2} \sum_{p=1}^{P} (\mathbf{r}_i^{(p)} - \mathbf{r}_i^{(p+1)})^2 + \\
\frac{1}{P} \sum_{p=1}^{P} \mathcal{W}_{classical}(\mathbf{r}_1^{(p)}, ..., \mathbf{r}_{N_Q}^{(p)}) \quad (3)
$$

where P is the number of beads in each polymer, N_Q is the number of "quantum" atoms and $\mathbf{r}_i^{(p)}$ is the position of the pth bead of atom i (noting that $\mathbf{r}_i^{(P+1)} = r_i^{(1)}$). $\mathcal{W}_{classical}$ is the normal, classical potential of the system, which will be a function of the pth copy of all the quantum particles as well as the coordinates of the "classical" particles. It should be emphasized that a dynamics simulation with the potential of eq 3 does not give the dynamics of a real physical system—it is only valuable as a way of calculating the ensemble averages for the corresponding quantum system.

It is straightforward to implement the above effective potential for use with a normal MM or QM/MM potential. The only major difference between the two implementations is that, in the hybrid potential case, P quantum mechanical calculations, instead of one, need to be done per energy or force evaluation (i.e., per step in a minimization or molecular dynamics calculation) which increases the simulation time needed considerably. In principle, it could be possible to use Car−Parrinello-like approaches to propagate the dynamics of the P copies of the wave function,[45−47] but in practice, we have found full self-consistent field calculations at each step to be sufficiently efficient.

We calculated the PMF for step a using the path integral procedure making the atoms HH-Y408, OH-Y408, and OE2-E275 quantum mechanical with 16 copies of each (i.e., $P = 16$). We also redefined the reaction coordinate in terms of the centroids of the polymers, i.e.,

$$
\xi_{rmRC1}^{PI} = \left| \left(\frac{1}{16} \sum_{i=1}^{16} \mathbf{r}_{OE2}^i \right) - \left(\frac{1}{16} \sum_{j=1}^{16} \mathbf{r}_{HH}^j \right) \right| \quad (4)
$$

Each molecular dynamics simulations was performed for 5 ps with data collection occurring in the last 4.5 ps of the simulation.

4. Ab Initio Calculations. To test the validity of the semiempirical AM1 QM approximation, we performed some single-point energy calculations with ab initio Hartree−Fock (HF) and density functional theory (DFT) methods. These calculations were done either with our ab initio QM/MM hybrid potential program[48] or with the program JAGUAR.[49] We employed the basis sets 6-31G** and 6-311G++**[50] and, for the DFT calculations, the B3LYP functional.[51] All ab initio calculations were done in the presence of the charges of the MM atoms to be directly comparable with the semiempirical hybrid potential results.

Results

1. The Free Molecular Dynamics Simulation. In the simulation with no constraints on the atoms of the two central zones, the hydrogen, HH, of Y408 formed a bond with atom OE2 of E275 but remained hydrogen-bonded to OH-Y408. This occurred very rapidly after ∼100 fs of dynamics. Shortly afterward, at ∼1 ps, the oxygen atom of tyrosine came as close as 1.45 Å to the C2 atom of the oxocarbonium intermediate, which is the distance corresponding to a covalent bond, and the hybridization of the C2 atom changed from sp[2] to sp[3]. While we realize that a single simulation is by no means representative, it had been thought unlikely that a covalent bond between the C2 atom and the tyrosine oxygen could occur due to their large separation (∼2.8 Å), even though the phenolate anion was supposed to stabilize the oxocarbonium's positive charge.[27] On the contrary, this simulation, like our earlier reaction path studies,[21] showed that the formation of the covalent bond can occur quite easily. How easily will become clear from the results of the free-energy calculations.

2. Formation of the Covalent Intermediate: Reaction I. The formation of the covalent intermediate involves the cleavage of one covalent bond and the formation of two others, as indicated in Table 1. We have treated it as involving two steps: (a) the transfer of the side-chain hydrogen of Y408 onto the carboxylic oxygen of E275 (reaction coordinate, RC1) and (b) the attack of the side-chain oxygen of Y408 on the C2 atom of the intermediate (reaction coordinate, RC2). While the lowest energy path on the free-energy surface could involve a concerted

(43) Feynman, R. P.; Hibbs, A. R. *Quantum Mechanics and Path Integrals*; McGraw-Hill: New York, 1965.

(44) Chandler, D.; Wolynes, P. G. *J. Chem. Phys*. **1981**, *74*, 4078−95.

(45) Car, R.; Parrinello, M. *Phys. Rev. Lett*. **1985**, *55*, 2471−4.

(46) Tuckerman, M. E.; Berne, B. J.; Martyna, G. J.; Klein, M. L. *J. Chem. Phys*. **1993**, *99*, 2796−808.

(47) Tuckerman, M. E.; Marx, D.; Klein, M. L.; Parrinello, M. *J. Chem. Phys*. **1996**, *104*, 5579−88.

(48) Amara, P.; Volbeda, A.; Fontecilla-Camps, J.; Field, M. J. *J. Am. Chem. Soc*. **1999**, *121*, 4468−77.

(49) Jaguar 3.5, Schrödinger, Inc., Portland, OR, 1998.

(50) Hehre, W. J.; Radom, L.; Schleyer, P. v. R.; Pople, J. A. *Ab Initio Molecular Orbital Theory*; J. Wiley & Sons: New York, 1986.

(51) Becke, A. D. *Phys. Rev*. **1988**, *A38*, 3098. Becke, A. D. *J. Chem. Phys*. **1993**, *98*, 1372−7. Becke, A. D. *J. Chem. Phys*. **1993**, *98*, 5648.

Intermediates in the Viral Neuraminidase Reaction

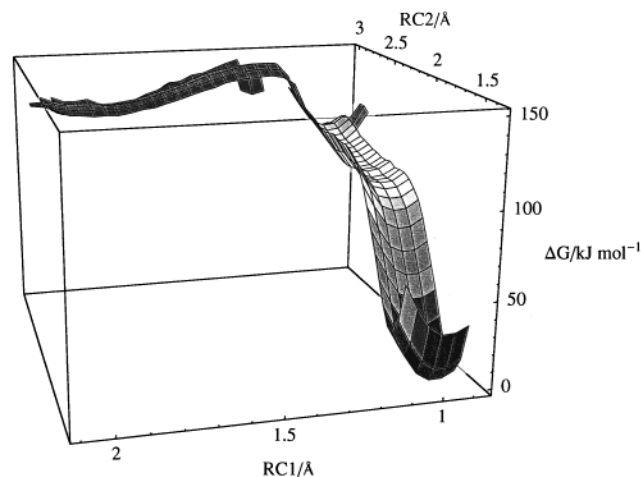*J. Am. Chem. Soc., Vol. 121, No. 41, 1999* 9699

Figure 6. Two-dimensional free-energy profile for the formation of the covalent intermediate via reaction I. In this figure and the subsequent ones, the reaction coordinates, whose definitions were given in Table 1, are in angstroms and the free energies are in kilojoules per mole.
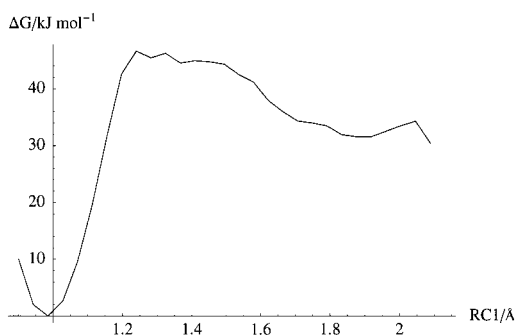

Figure 7. Free-energy profile for step a of reaction I determined from the path integral simulation. The barrier height for deprotonation of the tyrosine is found by following the profile from right to left.

Figure 8. Two-dimensional free-energy contour map of reaction II in which the C2 atom of the covalent intermediate is attacked by a water molecule which is deprotonated by D148. The contours of the map are at 10 kJ mol^{-1} intervals, and the lowest energy path between the two minimums is marked with a dotted line.

movement along a combination of these two coordinates, it became obvious from exploratory calculations that the actual mechanism was stepwise with step a occurring before step b. Thus, the two-dimensional free-energy profile shown in Figure 6 was calculated by varying RC1 between 0.9 and 2.0 Å, with RC2 fixed at its crystal structure value of 2.785 Å, and then keeping RC1 fixed at its minimum energy value of 0.97 Å, which corresponds to a covalent bond between OE2-E275 and HH-Y408, and varying RC2 between 1.2 and 2.9 Å. Step a has a relatively small barrier of 22 kJ mol^{-1} while step b is barrierless and formation of the covalent intermediate occurs spontaneously. The covalent intermediate is ∼120 kJ mol^{-1} more stable than the starting structure.

To estimate how much quantum effects would reduce the barrier for step a (and concomitantly the other hydrogen transfers we were studying) we performed a path integral simulation in which the hydrogen and the two oxygens most intimately involved in the reaction of step a were treated as quantum particles. The resulting free-energy profile is shown in Figure 7, whence it can be seen that the barrier is reduced by ∼6 kJ mol^{-1} from 22 to 16 kJ mol^{-1}. This is typical of the reductions that have been observed in a similar study of a hydrogen transfer using MM potentials.[52]

3. Hydroxylation of the Covalent Intermediate: Reaction II. To study the hydroxylation of the covalent intermediate by a water molecule we defined two reaction coordinates: RC3, which is the distance between OD1(D148) and the H2 atom of
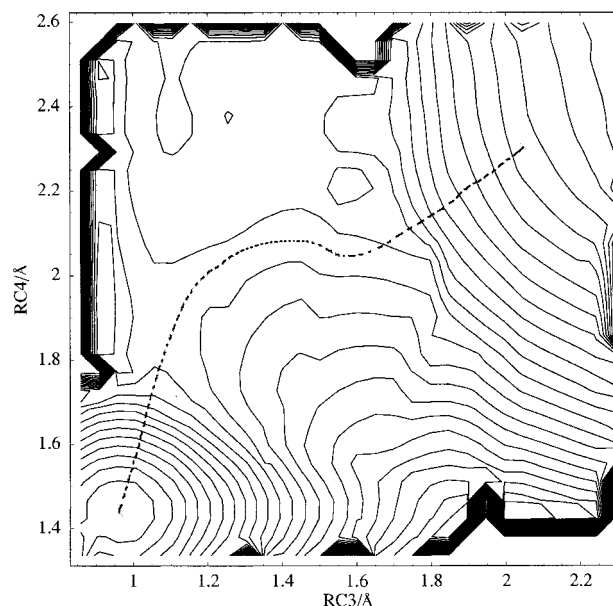
the water molecule, and RC4, which is the distance between the water oxygen atom and the C2 atom of the covalent intermediate. This reaction, together with the one to be described next, used the model in which there were 73 atoms in the QM region. The lowest energy path for this reaction involves concerted changes in both reaction coordinates, which meant that we had to calculate the full two-dimensional free-energy surface. The surface is displayed in Figure 8 and marked upon it, as a dotted line, is the lowest energy pathway. The barrier to the reaction is high, ∼110 kJ mol^{-1}, although there is little difference in energy between the two end states. Although the reaction is concerted, it is the transfer of the hydrogen from the water to the aspartate oxygen that occurs ahead of the formation of the bond between the water oxygen and intermediate C2 atoms.

4. Hydrogenation of the Tyrosine: Reaction III. Although the fact that the model we used to study reaction II could have allowed the tyrosine oxygen to recapture its hydrogen from E275, this did not occur in any of our simulations. This meant that it was necessary to add a third step, reaction III, to complete the hydroxylation reaction, which involved a hydrogen transfer between the protonated E275 and the phenolate oxygen of Y408. To compute this free-energy profile, we varied the reaction coordinate, RC5, which was the distance between the tyrosine oxygen and the hydrogen, while keeping the distance between the tyrosine oxygen and the C2 atom of the intermediate, RC6, fixed at 2.4 Å. The free-energy profile for this reaction, shown in Figure 9, has a barrier of ∼40 kJ mol^{-1} and results in a destabilization of ∼9 kJ mol^{-1}. That the barrier for this transfer is higher than that for step a is not surprising given that there is no longer a stabilizing positive charge at the C2 atom of the sialic acid product.

5. Hydroxylation of the Oxocarbonium Intermediate: Reaction IV. Our evaluation of the free-energy profiles for the hydroxylation of the oxocarbonium intermediate by a water molecule used a model with 47 atoms in the QM region. The reaction coordinates that we used are similar to those for reaction II, the major difference being the use of the compound reaction

(52) Hinsen, K.; Roux, B. *J. Chem. Phys.* **1997**, *106*, 3567−77.
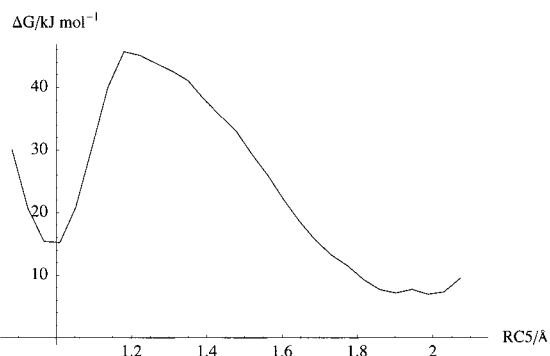
Figure 9. Calculated free-energy profile for the transfer of the hydrogen from E275 to the Y408 oxygen (reaction III). The barrier height for formation of the protonated tyrosine is found by following the profile from right to left.
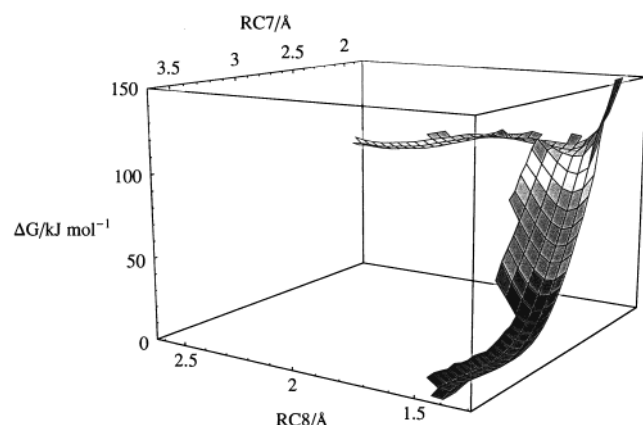

Figure 10. Two-dimensional free-energy profile for the hydroxylation of the sialosyl cation via reaction IV.

coordinate, $d_1 + d_2$, to describe the transfer of a hydrogen from the water molecule to the carboxylic oxygen of D148. We chose this compound form because we did not want to prejudge which hydrogen would leave the water molecule. As it turned out, however, it was always the same hydrogen, H2, that departed and that was why in our study of reaction II (which was performed *after* reaction IV) we chose the simpler reaction coordinate. The full definitions of the reaction coordinates are given in Table 1, and the resulting two-dimensional and one-dimensional free-energy profiles are illustrated in Figure 10 and Figure 11, respectively.

The reaction occurs essentially stepwise. First, the water oxygen approaches the C2 atom of the intermediate (reaction coordinate RC8) with a barrier of ~12 kJ mol^{-1} at an oxygen-carbon distance of ~1.95 Å (see Figure 11a). The value of the reaction coordinate, RC7, throughout this stage of the reaction is 1.98 Å (equivalent to twice the hydrogen-oxygen bond distance in water). When RC8 has a value of 1.6 Å, the reaction becomes concerted with RC7 increasing as RC8 decreases from 1.6 to ~1.4 Å (equivalent to a single covalent bond length between carbon and oxygen). This second step in which water loses one of its hydrogens is barrierless (see Figure 11b). The formation of the sialic acid in reaction IV results in a free-energy gain of ~97 kJ mol^{-1}.

6. Ab Initio Results. Although the AM1 semiempirical method is often reliable, its results have to be verified with more sophisticated QM techniques. The results of the free-energy calculations given above show that the barrier-determining step for formation of the covalent intermediate is proton transfer from tyrosine to glutamate whereas for the direct hydroxylation of the oxocarbonium intermediate it is the approach of the water

oxygen to the intermediate's C2 atom. How accurate is the AM1 method in describing these reactions?

In a paper to evaluate the accuracy of AM1 for the calculation of proton affinities and deprotonation enthalpies, Dewar and Deiter[32] showed that the errors in the calculated deprotonation enthalpy for phenol, propanoic acid, and water were about −5.8, +23.4, and +90.0 kJ mol^{-1}, respectively. This indicates that the AM1 method will overly favor the formation of a phenolate anion in step a of reaction I because AM1 predicts the protonated glutamate residue to be too stable. Likewise, in step f of reaction IV, AM1 will prefer the water to keep a proton, and not transfer it to aspartate, because the stability of the hydroxide ion is severely underestimated.

As an aside, we note that some workers have modified the parameters in the AM1 potential model to compensate for problems of this type.[53,54] In general, we do not favor this approach because it reduces the generality of the AM1 model. It also seems to us that if a reparametrization of the potential energy function is going to be undertaken it could be more effectively done on simpler and more computationally efficient functions such as those of the empirical valence bond type.[55]

Use of ab initio calculations to correct for the AM1 results is not entirely straightforward and we have tried several approaches. For the purposes of this paper, we show the results of two sets of calculations done on the barrier-determining steps mentioned above, i.e., step a of reaction I and step g of reaction IV. These calculations were performed as follows:

(1) A structure for each pathway, resulting from the dynamics simulations used for the free-energy calculations, was selected from near the top of the barrier (Figures 6 and 11a, respectively).
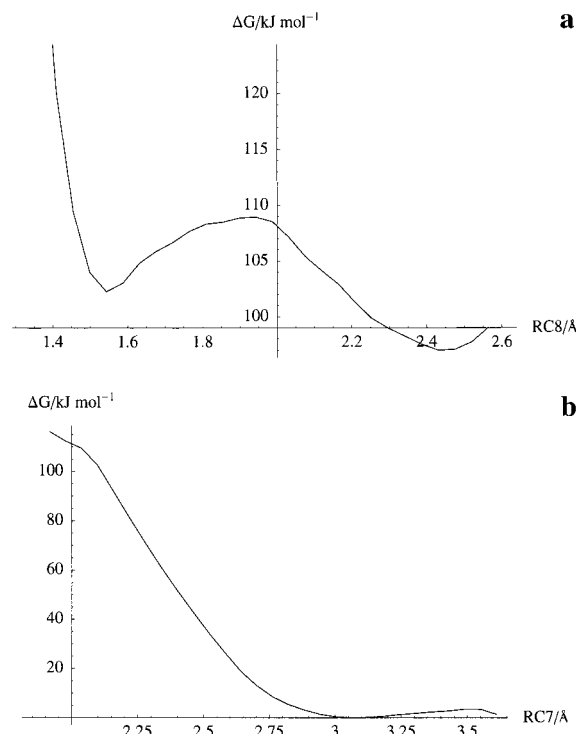

Figure 11. (a, b) One-dimensional profiles of the free-energy changes for steps g and f, respectively, of reaction IV. Production of the product proceeds by following the profile in (a) from right to left and that in (b) from left to right.

(53) Rossi, I.; Truhlar, D. G. *Chem. Phys. Lett.* **1995**, *233*, 231−6.

(54) Bash, P. A.; Ho, L. L.; MacKerell, A. D., Jr.; Levine, D.; Hallstrom, P. *Proc. Natl. Acad. Sci. U.S.A.* **1996**, *93*, 3698−703.

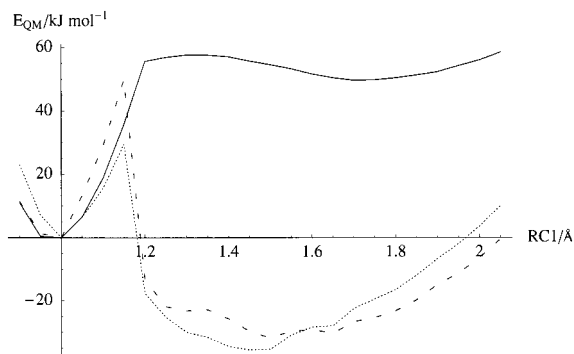(55) Warshel, A. *Computer Modeling of Chemical Reactions in Enzymes and Solutions*; J. Wiley & Sons: New York, 1991.

Intermediates in the Viral Neuraminidase Reaction

J. Am. Chem. Soc., Vol. 121, No. 41, 1999 9701

Figure 12. QM energies for the structures along the minimized pathway for step a of reaction I: AM1, solid line; HF, dashed line; DFT, dotted line.
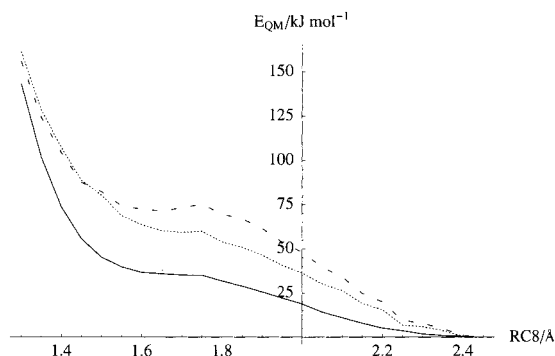

Figure 13. QM energies for the structures along the minimized pathway for step g of reaction IV: AM1, solid line; HF, dashed line; DFT, dotted line.

(2) These two structures were minimized with the semi-empirical hybrid potential and very strong harmonic constraints ($k_i \sim 100\,000$ kJ mol^{-1} Å^{-2} in eq 1) to keep the reaction coordinate variables at their barrier-top values. These values were RC1 = 1.25 Å and RC2 = 2.785 Å for step a and RC7 = 1.98 Å and RC8 = 1.95 Å for step g.

(3) Starting from the minimized structures of step 2, new structures were obtained by both incrementing and decrementing the reference values of the reaction coordinates RC1 and RC8 by 0.05 Å and then reminimizing. This procedure was repeated until a series of minimized structures was obtained that spanned the complete range of the reaction coordinates, RC1 and RC8.

(4) The energies of each of the minimized structures along the pathway were obtained using ab initio HF and DFT calculations with the 6-311G++** basis set. Note that the same number of QM atoms were treated in both the semiempirical and ab initio calculations (i.e., 63 QM atoms for step a and 47 QM atoms for step g) and that the charges of the MM atoms were included in the ab initio QM calculations in the same way as they were in the semiempirical calculations.

The QM energies resulting from these calculations for reaction coordinates RC1 and RC8 are shown in Figures 12 and 13, respectively. Figure 12 clearly illustrates the problem that AM1 has in reproducing the deprotonation enthalpy of the glutamate residue. Whereas the barriers to the proton transfer on going from the glutamate are in reasonable agreement for the three methods, protonated tyrosine is much less stable relative to protonated glutamate for the AM1 model than for the ab initio methods (the difference is of the order of 80 kJ mol^{-1}). This implies that the barrier to proton transfer will be significantly higher than predicted by the free-energy calculations and that, as a result, the covalent intermediate will be more difficult to form.

In contrast to the results for RC1, all three curves for RC8 in Figure 13 show a similar behavior. The QM energies increase steadily as the value of the reaction coordinate is reduced from 2.5 to ~1.75 Å; there is a slight well between 1.7 and 1.6 Å and then the energy increases again. Whereas the qualitative behavior of the curves is the same, the HF and DFT energies are larger, which would again indicate that the barrier predicted in the free-energy calculations is too low. The effect is by no means as large though as it is for step a.

A couple of comments are in order concerning the ab initio results. First, the ab initio calculations were performed for a minimum-energy pathway optimized with the AM1 potential. Thus, while it is probable that the barrier determined by AM1 for step a is too small, it is likely that the errors will not be as large as those indicated by the energy differences between the AM1 and ab initio curves in Figure 12. This is because optimization of the path with an ab initio hybrid potential could well produce lower barriers. Second, a valid question arises, given the differences in the AM1 and ab initio results, as to whether the reaction mechanisms at these different levels of theory remain the same.

To answer this last question, we have carried out further ab initio calculations of the type discussed above and, although we do not present any further results here, we summarize what we find as follows:

(1) Reaction I still occurs in a stepwise fashion but the value of the reaction coordinate RC2 at which the proton transfer takes place is smaller, at RC2 ~2.4 Å as opposed to ~2.8 Å, and the barrier is reduced to ~50 kJ mol^{-1} at both the HF and DFT levels of theory as compared to the values in Figure 12.

(2) A covalent intermediate will form whenever the tyrosine loses its proton to the glutamate. This is in contradiction to proposals in the literature, which state that it is the tyrosine anion that stabilizes the oxocarbonium intermediate because the distance of 2.8 Å between the tyrosine oxygen and the C2 atom of DANA observed in the crystal structure is too large for a covalent bond to form.[17]

(3) The mechanism for reaction IV is essentially unchanged. This is partly due to the fact that the deprotonation enthalpy of water is much larger than that of aspartic acid, even though the stability of the hydroxide ion is underestimated by the AM1 method.

Discussion and Conclusions

In this paper, we have studied the active site of a viral neuraminidase using theoretical techniques. This is not the first such study—calculations have already been employed for computer-aided design of anti-influenza drugs and the prediction of binding affinities in neuraminidase,[8,56] to find the possible location of the water molecule neighboring the C2 atom of a sialic acid bound in the active site[15] and to investigate certain aspects of the reaction mechanism.[20,21]

The current work was motivated by an earlier study of ours[21] in which we showed that a covalent enzyme–intermediate complex could be formed during the catalytic reaction either directly from the reactant species or from the oxocarbonium intermediate that has been postulated to occur in the mechanism. The aim of this new work has been to try and establish how likely the formation of such a covalent complex is. As such we have started with the oxocarbonium intermediate (which can be characterized as a true intermediate) and examined two

(56) Taylor, N. R.; Cleasby, A.; Singh, O.; Skarzynski, T.; Wonacott, A. J.; Smith, P. W.; Sollis, A. L.; Howes, P. D.; Cherry, P. C.; Bethell, R.; Colman, P.; Verghese, J. *J. Med. Chem.* **1998**, *41*, 798−807.
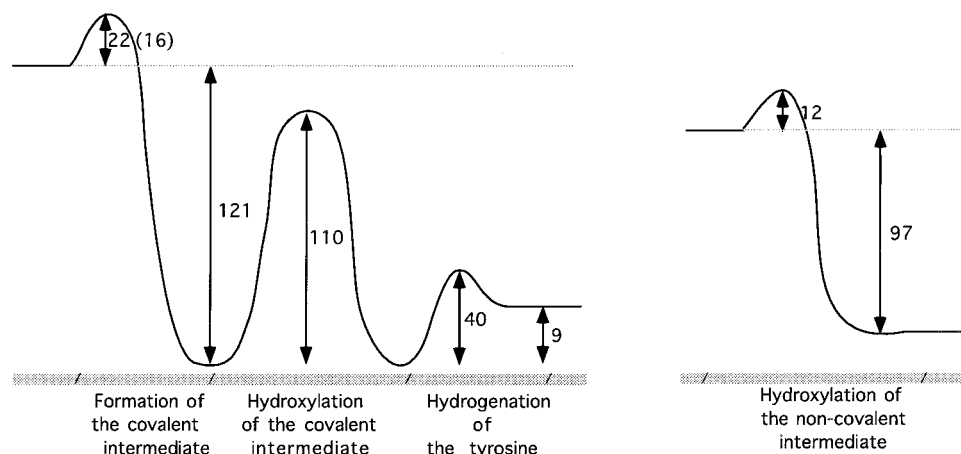
Figure 14. Schematic diagram of the free-energy values in our reaction schemes for the formation of the sialic acid product from the oxocarbonium intermediate via a covalent intermediate (left plot) or by direct attack by water (right plot).

competing pathways for formation of the sialic acid product—one via a covalent intermediate and one via direct hydroxylation by water. A schematic of the free-energy values that we obtained for each of these two mechanisms is shown in Figure 14.

The first thing to point out about the two mechanisms is that the overall free-energy changes for the two reactions, which should, of course, be the same, differ by $\sim$15 kJ mol^{-1}. We consider this to be a reasonable agreement, given that the QM/MM partitionings for the free-energy calculations of different stages of the overall reaction were not the same, and allows us to have confidence in the internal consistency of the hybrid potential.

As far as which mechanism is favored, it is clear that the pathway for the direct hydroxylation of the oxocarbonium intermediate by a water hydrogen-bonded to D148 has the lower energy barrier—12 as opposed to 22 kJ mol^{-1}—although the inclusion of quantum dynamical effects will reduce both these values. A path integral simulation of the barrier-determining step in the formation of the covalent intermediate led to a barrier reduction of $\sim$6 kJ mol^{-1}, but a smaller reduction would be expected for the direct hydroxylation reaction because the barrier-determining step does not involve a hydrogen transfer. Nevertheless, even with these reductions, it appears that the direct-attack pathway will be the preferred mechanism by of the order of 5−10 kJ mol^{-1}.

If the covalent intermediate were to be formed, our calculations indicate that its breakdown requires substantial energy barriers to be overcome—$\sim$130 kJ mol^{-1} to return to the oxocarbonium intermediate and 110 kJ mol^{-1} to produce sialic acid from hydroxylation by a water molecule. The last step, reaction III in Table 1, concerns only the side chains of the protein and so could occur after the sialic acid has left the active site and been replaced by water molecules.

There are a number of criticisms that can be made of the approach that we have taken. First, we are aware that the choice of our reaction coordinates is arbitrary and that the real reaction cannot be fully explained in terms of them. However, the energy barriers that we calculate will be upper bounds to the free energies for the reaction because the addition of extra coordinates can only lower the energy. Likewise, the calculation of the free-energy differences between end states is independent of the path taken and so these values should be valid. Another criticism that can be made is the use of the AM1 semiempirical model to describe the reaction process. To estimate its precision for our reaction, we undertook ab initio calculations as checks and found that, indeed, the AM1 method does tend to favor the mechanism in which the covalent intermediate is formed. This does not qualitatively alter our conclusions although it does mean that the covalent intermediate is more difficult to form than the AM1 calculations suggest. The ab initio calculations also imply that a protonated tyrosine stabilizes the oxocarbonium intermediate and not the anion as has been proposed elsewhere.[17]

In summary, our calculations indicate that the neuraminidase reaction does not pass preferentially via a covalent intermediate, although the difference between the free-energy barriers for the pathway in which such an intermediate occurs and in which the product is formed directly by an attack by a water molecule may not be all that large. Thus, it might be possible, with suitable substrates, to bias the neuraminidase reaction toward the formation of a covalent intermediate. If so, this may provide an additional route for the design of potent neuraminidase inhibitors that could act as anti-influenza drugs.